FLOW CHARACTERIZATION OVER SQUARE RIB

Sachu S Soman, Santosh Kumar Singh*
School of mechanical engineering SRM Institute of science and technology Kattankulathur
Chennai 603203
Email: santoshk@srmist.edu.in

Abstract
This research provides a numerical verification of unsteady reattaching turbulent flow past a two-dimensional square rib that mimics experimental conditions documented in earlier literature [1]. The simulation was conducted at a Reynolds number of 13,200 based on the rib, using the Reynolds-averaged Navier–Stokes (RANS) equations with the k–ω shear stress transport (SST) turbulence model. The computational domain is specified with a relative channel height of δ/H = 0.75 to match experimental setups. The simulation correctly reproduces important flow features such as flow separation, recirculation, and reattachment below the rib. Results such as mean velocity profiles and turbulence properties are compared to experimental data for verification. The computed flow structure reveals a good correlation with experimental evidence, testifying the applicability of the SST model in simulating rich turbulent behaviour in ribbed channel flows. This research affirms the employment of RANS-based methods for the practical modeling of turbulent flow in engineering.
Keywords: Computational fluid dynamics, RANS, k–ω shear stress.

1. Introduction

Turbulent flows with separation and reattachment are common in numerous engineering applications, including heat exchangers, gas turbines, and aerodynamic surfaces. Surface-mounted obstacles, such as square ribs, greatly affect the flow characteristics and create complex phenomena such as flow separation, recirculation zones, and reattachment points. The comprehension of these flow behaviors is essential to optimize design and maximize performance in engineering systems [2]. The research on unsteady separated and reattaching turbulent flows over two-dimensional square ribs has attracted considerable attention due to its application in predicting flow-induced vibrations, augmentation of heat transfer, and drag reduction. Experimental measurements, including those performed in[1], have contributed to a better understanding of the spatio-temporal behavior of such flows, including the development of shear layers, vortex shedding, and reattachment zone dynamics.

Some researchers have examined the flow over square ribs with both experimental and numerical methods. Liu and Sung [1] made synchronized wall-pressure and velocity fluctuation measurements to examine the separated and reattaching turbulent flow over a two-dimensional square rib. The results showed the existence of large-scale vortical structures and a thin region of reverse flow above the rib, and the reattachment point was found to be downstream at about x/H = 9.75.Gu et al. [3] conducted a numerical simulation based on Large Eddy Simulation (LES) to study separating–reattaching flow over a surface-mounted rib and the associated instability. They detected the occurrence of Kelvin–Helmholtz (K-H) instability in the shear layer and the phenomenon of vortex pairing, adding insights into flow dynamics in the separation zone.

The detailed visualizations of the separated and reattaching turbulent flow around a surface-mounted square cylinder were given by Chun et al. [4] using time-resolved Particle Image Velocimetry (TR-PIV) measurements. Their results showed the importance of large-scale vortical structures in contributing to the fluctuating flow field and stressed the need for accurate predictions to capture unsteady flow features.

The simulation of unsteady separated and reattaching turbulent flows over surface-mounted obstacles, like ribs, is still a major challenge in computational fluid dynamics (CFD). Such flows are marked by intricate phenomena like boundary layer separation, shear layer formation, vortex shedding, and turbulent reattachment, which present major challenges to numerical prediction with accuracy. Menter's [5,6] k-omega Shear Stress Transport (SST) turbulence model is now a widely used method for such flows, its hybrid formulation which combines the virtues of k-epsilon and k-omega models. The current introduction considers the theoretical background of the SST model, its usage in separated flows, and why its performance has been verified when simulating flow over a two-dimensional square rib using ANSYS CFD.

Separated flows over bluff bodies are found in many engineering situations, such as heat exchanger tubes, turbomachinery blades, and building aerodynamics [7,8]. The flow over a square rib provides a canonical example for the investigation of separation dynamics because of the sharp pressure gradients at the leading edge of the rib and the subsequent development of a recirculation zone downstream. Precise prediction of reattachment length, pressure recovery, and distribution of turbulent kinetic energy is vital to maximize thermal performance in ribbed channels and reduce drag in aerodynamic setups. These parameters have been measured through experimental work, but it is still tough to numerically validate them considering the inherent flaws in turbulence modeling in capturing anisotropic turbulence and unsteady vortex structures [9].

Reynolds-Averaged Navier-Stokes (RANS) is the foundation for the majority of industrial CFD simulations because of its computational efficiency. Early eddy-viscosity models such as the standard k-epsilon model had difficulties in near-wall resolution and adverse pressure gradient flow, tending to overestimate turbulent stresses and underestimate separation zones. The k-omega model remedied some shortcomings by enhanced near-wall treatment but was still freestream-condition-sensitive. Menter's [5] SST model brought with it two primary innovations, one is blending function (F1): Seamless transitions between k-epsilon formulation in the outer region and k-omega near walls second one is Viscosity limiter: Prevents overprediction of turbulent viscosity in regions with strong shear, crucial for separation prediction[5,6].

The transport equations for turbulent kinetic energy (k) and specific dissipation rate (ω) are

$$\frac{D}{Dt}(\rho k) = \nabla.(\rho D_k \nabla_k) + \rho G - \frac{2}{3}\rho k(\nabla.\mathrm{u}) - \rho\beta^* \omega k \quad (1)$$

$$\frac{D}{Dt}(\rho\omega) = \nabla.(\rho D_\omega \nabla_\omega) + \frac{\rho\gamma G}{v} - \frac{2}{3}\rho\gamma\omega(\nabla.u) - \rho\beta\omega^2 - \rho(F_1 - 1)CD_{k\omega} \quad (2)$$

ANSYS Fluent's pressure-based solver was used second-order spatial discretization and bounded second-order implicit transient formulation. Boundary conditions will simulate wind tunnel test, with 5% turbulence intensity and hydraulic diameter defined at inlet. The computational domain is 20H upstream and 54H downstream (H = rib height) to reduce boundary influence. The major validat ion parameters are$Lr/H=f(Re,$turbulence model). where Lr is reattachment length, and Re is Reynolds number based on rib height. This thorough validation fills gaps in current literature by systematically assessing the SST model performance for a benchmark separated flow case, offering insights for industrial applications demanding precise separation prediction.

2. Numerical Procedure

2.1.Numerical model

The k-ω Shear Stress Transport (SST) two-equation eddy-viscosity turbulence model, formulated by F.R. Menter in 1994, is a popular two-equation eddy-viscosity model used in computational fluid dynamics (CFD). The model's strength lies in the convergence of the k-ω and k-ε models' individual strengths to overcome their respective weaknesses. The k-ω model is strong in the near-wall region and is capable of properly resolving the sub-viscous layer, whereas the k-ε model works well for predicting away-from-wall flow behavior. The SST model combines these two models using a switching function through blending functions, which allows smooth transition between the models based on the flow region.

$D/D_t(\rho k)=\nabla\cdot(\rho Dk\nabla k)+\rho G-2/3\rho k(\nabla\cdot\mathbf{u})-\rho\beta^{*}\omega k+S_k$ (3)

Where D_kDiffusion coefficient for k,G isthe Production term related to shear stress, and $k$isthe Source term$\beta*$ Model constant.

The governing equations of the k-ω SST model are formulated based on the transport of turbulence kinetic energy (k) and specific dissipation rate (ω). The kequation includes its convection, diffusion, production, and dissipation, while theω also contains convection, diffusion, production, and destruction terms. The turbulent viscosity (μ) is determined with the use of a limiter to avoid excessive accumulation of turbulent kinetic energy in areas with negative pressure gradients or heavy acceleration. The limiter provides improved correlation with experimental results for separated flows.

One of the most important benefits of the k-ω SST model is that it can more accurately predict flow separation compared to conventional RANS models. It also handles adverse pressure gradient conditions well, and thus it is extremely well-suited for use in applications like external aerodynamics (e.g., air foil or wing flow). Nevertheless, the model is capable of generating high turbulence levels in areas of high normal strain, like stagnation points, although this impact is weaker than in conventional k-ε models.

2.2.Model geometry and boundary conditions

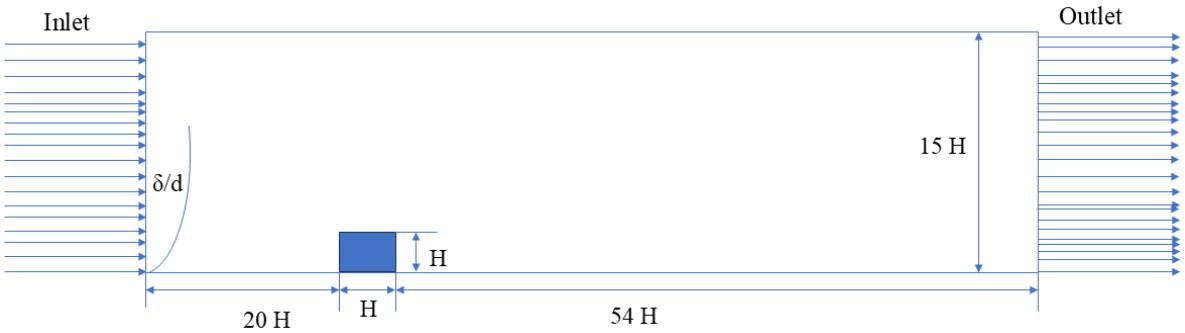

Fig 1. Schematic diagram of geometry.

For the given H = 20 mm, the model is a two-dimensional channel that is 300 mm in height and 1500 mm in length, with a square rib having height and width 20 mm on the bottom wall. The position of the rib is 400 mm downstream from the inlet and 1080 mm upstream from the outlet. The inlet is provided with a uniform velocity of U_0 = 10 m/s, and the Reynolds number R_{eH}= 13,200, and the ratio of boundary layer thickness to rib height (δ/H) is 0.75. The pressure outlet is specified at the outlet of the channel, velocity inlet is specified as inlet of the channel, whereas the top and bottom walls are provided with a no-slip boundary condition.

.

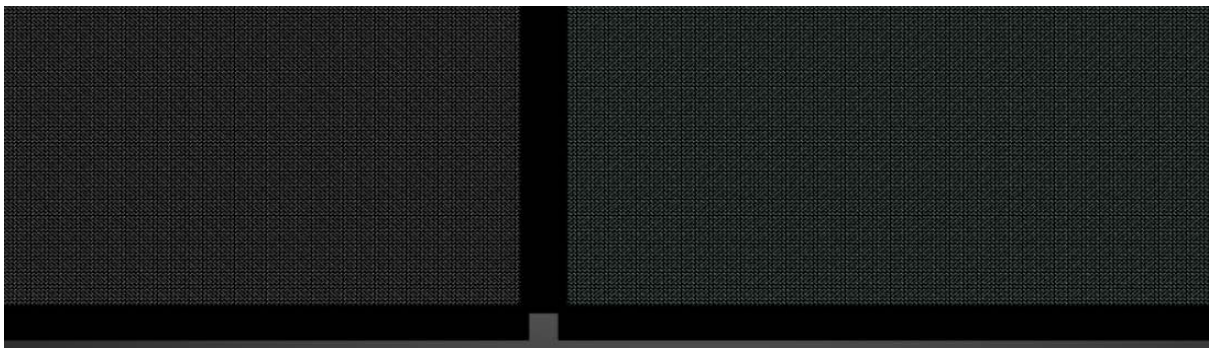

Fig 2: Schematic of the mesh of geometry

2.3.Grid Independence test

Case	Mesh	C_D	C_L
M1	38,755	1.1094	0.6303
M2	73,575	1.0258	0.6383
M3	98,533	1.0194	0.6283

Table1: Hydrodynamic quantities for different grids at R_{eH}= 13,200

To guarantee the reliability and accuracy of our hydrodynamic simulations, a grid independence test was performed with three different mesh densities: M1 with 38,755 elements, M2 with 73,575 elements, and M3 with 98,533 elements. The results, shown at a Reynolds number of 13,200, indicate a convergence of the hydrodynamic quantities with increasing mesh density. In particular, the drag coefficient (C_D) drops from 1.1094 for M1 to 1.0194 for M3, reflecting stabilization of the solution as the meshes are finer. Also, the lift coefficient (C_L) shows small changes, from 0.6303 for M1 to 0.6283 for M3, reflecting that the solution is not very sensitive to the mesh density above a certain level. This grid convergence behavior assures us that the numerical outcomes are not a function of the mesh size and are robust, thus establishing the grid independence of our simulations.

2.4.Numerical validation

The horizontal velocity profile from the current simulation with the use of the $k-\omega$ turbulence model and the experimental results of Liu et al. at Re = 13,200 with δ/H= 0.75 exhibits good agreement. The simulation data symbolized by the solid line closely aligns with experimental measurements shown as circles, tracing the trend and magnitudes of the peak velocities. Small discrepancies are seen in the vicinity of areas with steep gradients, which may be due to resolution and turbulence model approach differences. The $k-\omega$model properly captures smaller turbulent scales, which improves predictive precision for flow properties in such setups. This comparison highlights the consistency of numerical simulations in simulating experimental observations at high Reynolds numbers.

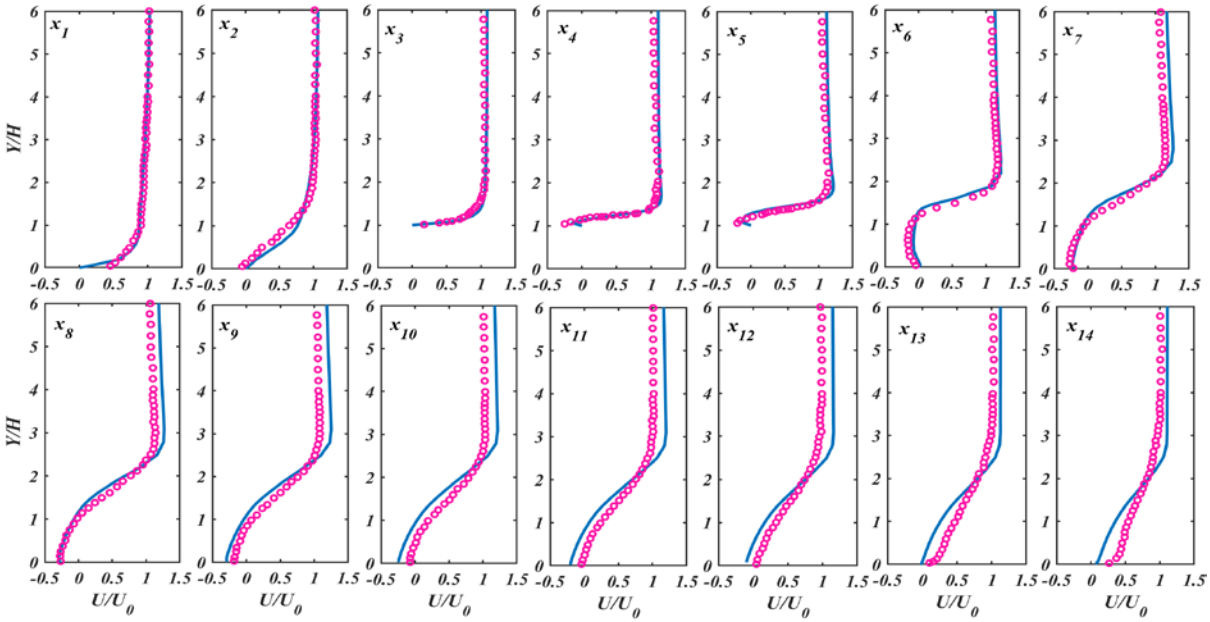

Fig 3. Comparison of the horizontal velocity profile of the present simulation (solid line) and the experimental data from Liu et.al. [1] (circles) at Re = 13,200 with δ/H = 0.75

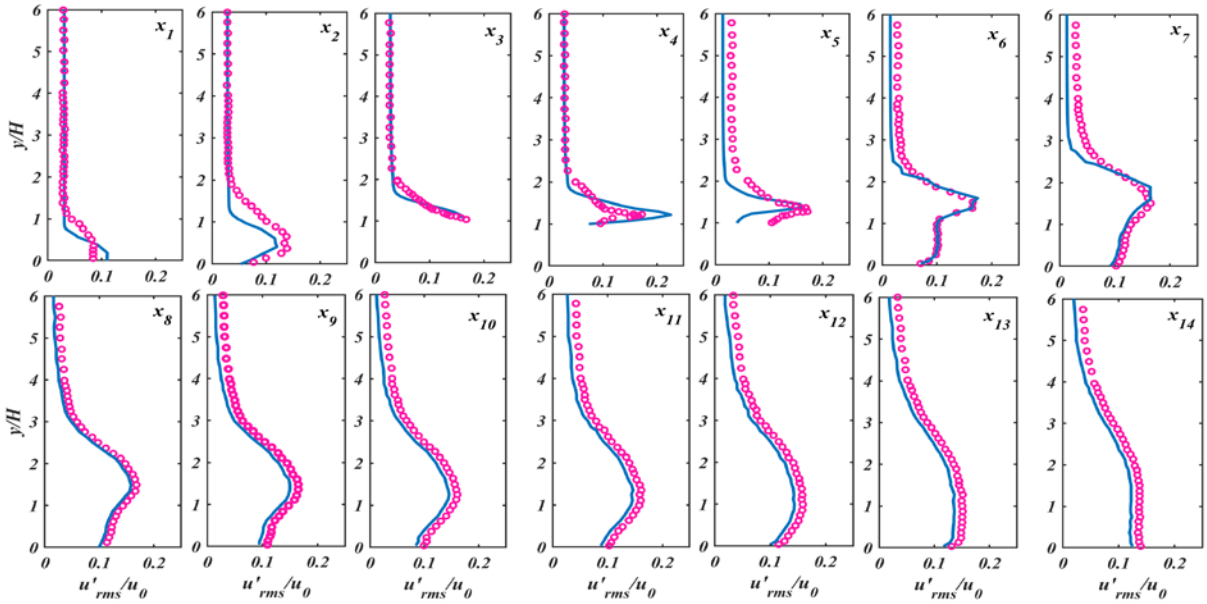

Fig 4. Comparison of the streamwise velocity fluctuation intensity of the present simulation (solid line) and the experimental data from Liu et.al. [1] (circles) at Re = 13,200 with δ/H = 0.75

The figure plots streamwise velocity fluctuation intensity from a $k-\omega$ SST simulation (solid blue lines) compared with experimental results of Liu et al. (2008) (magenta circles) at Re = 13,200 with δ/H = 0.75, for 14 streamwise locations. The graphs depict both simulation and experimental data depict low fluctuation intensities close to the wall, rising to a maximum, then falling further away from the wall. The $k-\omega$SST model captures the overall trend, particularly in the outer region, but underpredicts the maximum fluctuation intensity in the inner region at certain locations. The streamwise development of the fluctuation profiles is well-captured in general.

3. Result and Discussion

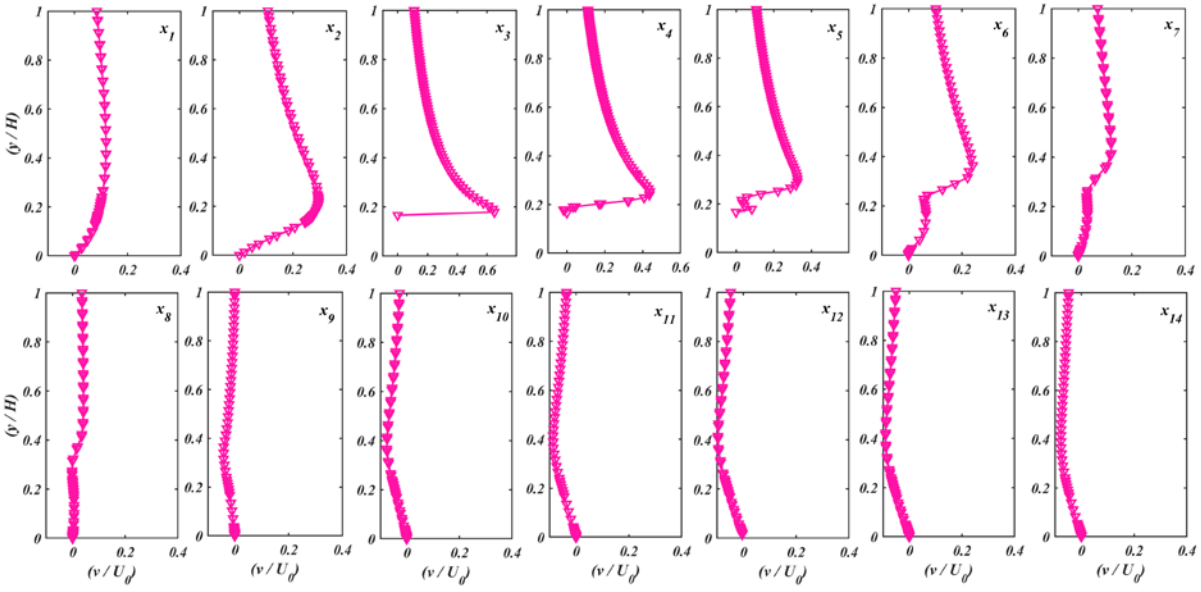

Fig.5 Normalized y velocity component

The plot shows a complete series of velocity profiles of the relationship between normalized y-velocity (v/U$_0$) along the x-axis and the normalized height (y/H) along the y-axis at 14 spatial points marked x$_1$ to x$_{14}$. The profiles trace the vertical component of velocity of what seems to be a fluid flow test, probably showing flow structure development in various positions of measurement.

For the top row (x$_7$ to x$_{14}$), profiles differences in shape and size. Profile x$_1$ has zero velocity at the lower edge, quickly rising to about 0.2 at about 20% of the normalized height before tapering off in a very steep profile with

little change in velocity with more height. Profile x shapes profile with velocity incrementally going up to about 0.3 at half-height before turning downwards. Profiles x x more elevated velocities trending further to the right (about 0.6 for x vertical flow components at these positions.

The shift to profiles x and move towards more S-shaped curves with inflection points at varying heights. This reflects complicated flow patterns with varying velocity gradients along the vertical direction. The highest normalized velocities in these profiles are still below 0.4, with most peak values at 20-40% of the channel height.

Bottom row (x x in the flow behavior. These profiles trend almost vertical and parallel to the y-axis, showing insignificant vertical velocity components at these positions. All bottom-row profiles exhibit close-to-zero normalized velocities across the full height, inferring the establishment of the flow pattern as dominantly horizontal with minor vertical activity.

This development from large vertical velocity components as in the initial profiles to nearly zero vertical flow in the subsequent stations probably accounts for the growth of a developing flow that finally settles into a more one-way oriented pattern. This kind of measurement is typical in boundary layer research, channel flow, or other confined flow conditions where initial complicated three-dimensional flow patterns slowly give way to more two-dimensional profiles as the flow develops downstream.

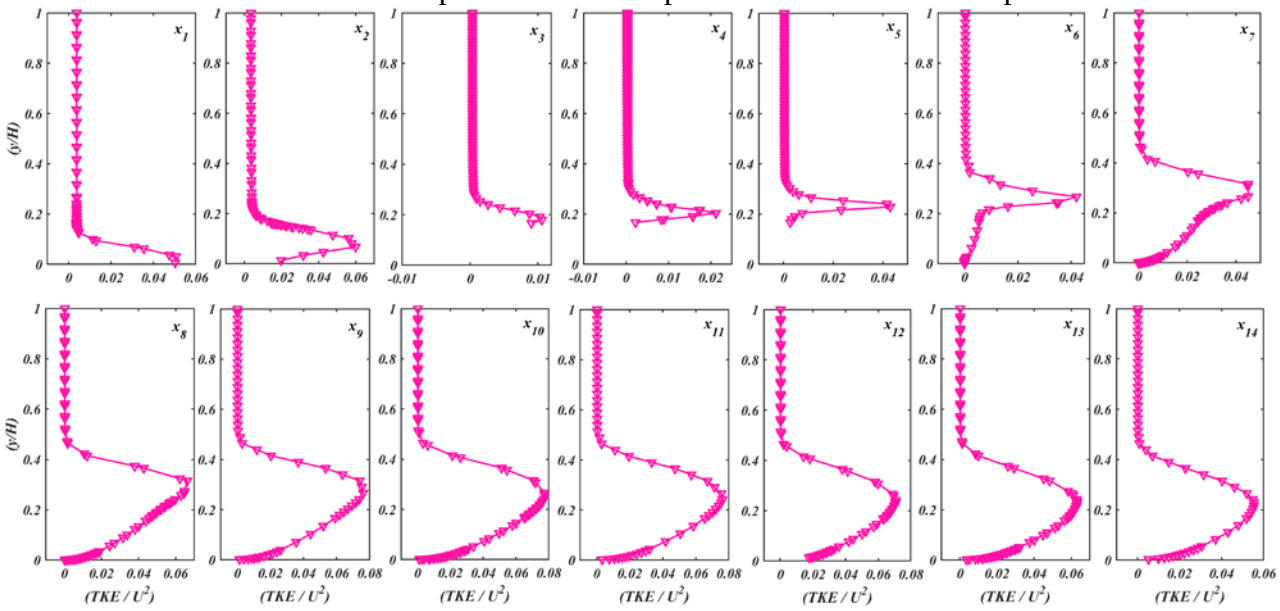

Fig.6 Normalized TKE

The figure provided shows the vertical profiles of normalized turbulent kinetic energy *(TKE/U²)* as a function of normalized height (y/H) at several streamwise locations along the flow over a two-dimensional square rib. As per the study referred to, the front end of the rib is at x_3 whereas the back end is between x_3 and x_5. At the leading edge (x_3), TKE is sharply peaked near the wall and rapidly decays with height, reflecting intense turbulence due to flow separation as the boundary layer encounters the rib's upstream face. This is consistent with the formation of a separated shear layer, which is a well-known feature in flows over surface-mounted obstacles As the flow progresses downstream (from x_3 to x_5), the TKE profile continues to be higher near the wall but spreads and moves upwards, reflecting the formation of a recirculation region and the development of the separated shear layer following the rib. The elevated TKE in this zone is due to high velocity gradients and vortex shedding, typical of reattaching and separated turbulent flows. More downstream (past x_5), the profiles of TKE reveal a diminution in values at the peaks and a less non-uniform distribution along the channel height, indicating the decreasing turbulence as flow reattaches to the wall and recovers towards equilibrium. This trend is consistent with experimental and computational observations that TKE is maximum in the recirculation region and then decreases as the turbulent structures get deformed and energy is lost he development of TKE profiles through the rib captures the basic physics of separation, vortex creation, and reattachment, with maximum

turbulence intensity right behind the rib and decreasing downstream as the flow redevelops. This is a characteristic of unsteady, separated, and reattaching turbulent flows over two-dimensional ribs.

Following x5, the normalized turbulent kinetic energy (TKE/U^2) profiles exhibit a clear development that is a consequence of the flow reattachment and recovery processes further downstream of the square rib. At x6 and x7, the TKE close to the wall is still high, yet the peak starts to move upwards and widen, which is indicative of continuing turbulence generation as the separated shear layer interacts with the wall and the recirculation zone continues. This high TKE is a characteristic of intense mixing and vortex activity common in the reattachment region.

Between x8 and x14, the TKE profiles slowly become more consistent across the channel height, and the maximum values reduce. This trend indicates that the turbulent structures produced by the rib are dissipating, and the flow is becoming a redeveloped turbulent boundary layer. The decrease in TKE and the smoothing of the profile suggest the loss of energy from large-scale eddies to lower scales via the turbulence cascade, ultimately producing more stable and less energetic flow downstream.

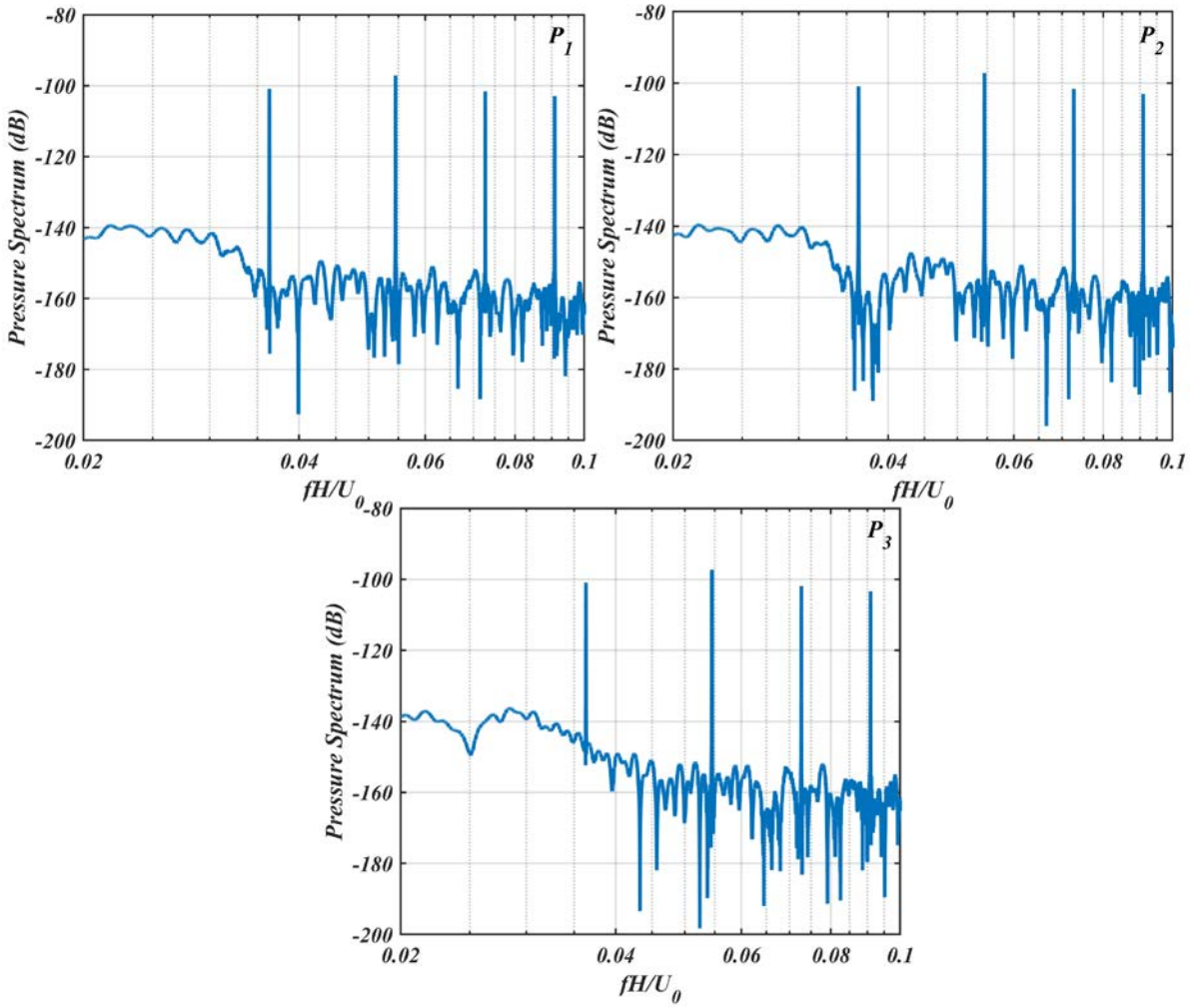

Fig. 7 Pressure Spectrum.

The spectrum of wall pressure at various points surrounding a square rib is significant and very enlightening with respect to the turbulent flow patterns and their influence on surface pressure fluctuations. The spectra at P1 (square rib leading point), P_2 (square rib midpoint), and P_3 (leading edge) are different. At P_1, the spectrum contains a wide band of frequencies with multiple dominant peaks, reflecting the existence of numerous she dding frequencies because of the reattachment and flow separation. The mid-rib site P_1 indicates a similar trend but with a different distribution of peak amplitudes, indicating the development of turbulent structures as they propagate over the surface of the rib. The

leading edge P_1 indicates the smaller amplitudes than other si tes. These peaks correspond to the shear layer instabilities. The analysis of these spectra enables us to understand the dynamic loading on the rib and the surrounding wall, which is significant to evaluate structural integrity and create effective noise reduction mechanisms.The slight differences in peak frequencies and amplitudes (about 0.01) between P_1, P_2, and P_4 are mostly caused by the changing nature of the turbulent flow as it interacts with the square rib. Flow separation occurs at the leading edge of the rib (P_1), which produces shear layer instabilities that create unique pressure fluctuations. As the flow travels along the surface of the rib towards P_2, these turbulent structures develop, with some being dissipated and others combining or strengthening, resulting in changes in the frequency and amplitude of the pressure peaks. Also, the point P_3, being at the front edge, has different boundary conditions and flow behavior than P_1 and P_2, which also contributes to the noted spectral differences. These slight changes represent the intricate interplay of the processes of turbulence, separation, and reattachment on the rib.

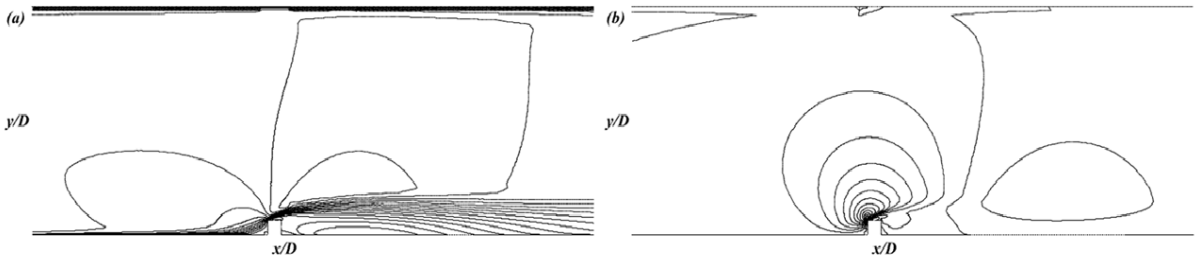

Fig.8: Horizontal(fig 8a) and vertical velocities(fig 8b)

The arrows depict the horizontal (a) and vertical (b) velocity components in a fluid flow, around therib constriction. For Figure 8a, horizontal velocity has a clear acceleration as the flow moves toward the obstacle, as represented by the densely packed streamlines. There is a stagnation point on the front edge where the flow splits. Downstream, the velocity profiles imply a growing boundary layer and possible wake formation with diminished horizontal velocity. Figure 3b shows the vertical velocity, with intense upward motion close to the leading edge followed by a return towards the centerline downstream. The areas of high vertical velocity coincide with flow separation and recirculation regions. These observations align with the findings of [10], who studied similar flow phenomena and emphasized the importance of understanding separation and reattachment processes for accurate modeling.

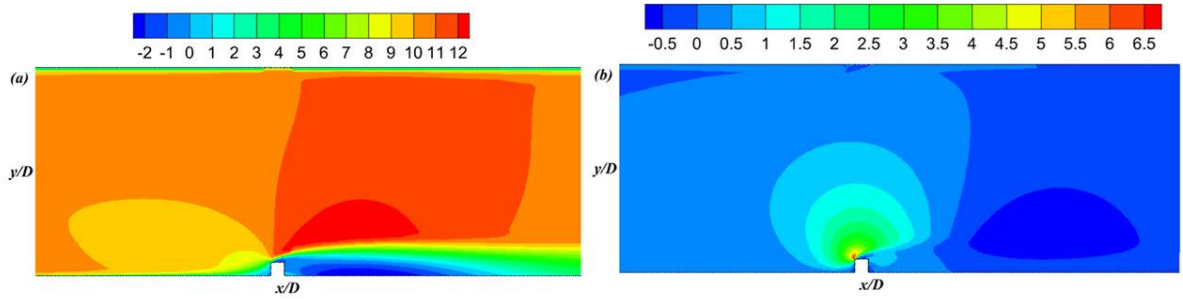

Fig.9: Horizontal(fig 9a) and vertical velocity (fig 9b) contour.

Fig. 9 shows fluid velocity behavior in terms of contour plots, with (a) representing horizontal velocity and (b) representing vertical velocity. In (a), the color variation surrounding the obstruction represents flow acceleration due to the smaller flow area, following mass conservation principles, while the dark area behind the obstruction represents a low-velocity wake resulting from flow separation and recirculation. Towards the walls, the reduction in horizontal velocity illustrates the existence of a boundary layer under viscous influence. Plot (b) illustrates vertical fluid movement with the color change above the barrier indicating upward flow deflection. Patterns downstream are likely to point towards vortex shedding, an unstable process where vortices shed off from alternately opposite sides of the obstruction. Symmetry in vertical velocity distribution suggests that flow deflection is balanced.

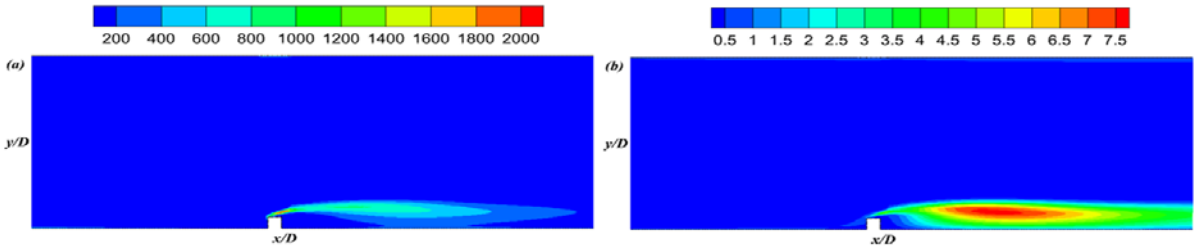

Fig.10: TDE (fig 10a) and TKE (fig 10b)contour.

The contour plots are showing the distribution of Turbulent Dissipation Energy (TDE) in Fig. 6a and Turbulent Kinetic Energy (TKE) in Fig. 10 b behind an obstacle at x/D = -1. TDE is the rate of turbulent kinetic energy dissipation into thermal internal energy, with maximum values found in the wake region because the shear layer detaching from the obstacle creates strong turbulence; TDE diminishes downstream as turbulence fades and disperses vertically. Likewise, TKE, or the mean kinetic energy of turbulent eddies, is most prominent in the wake region because of the instability of the shear layer, declining downstream as turbulent eddies dissipate energy, and also spreading vertically; these graphs illustrate the turbulence intensity and distribution, illustrating energy transfer from the mean flow to turbulent eddies (TKE) and dissipation into heat (TDE).

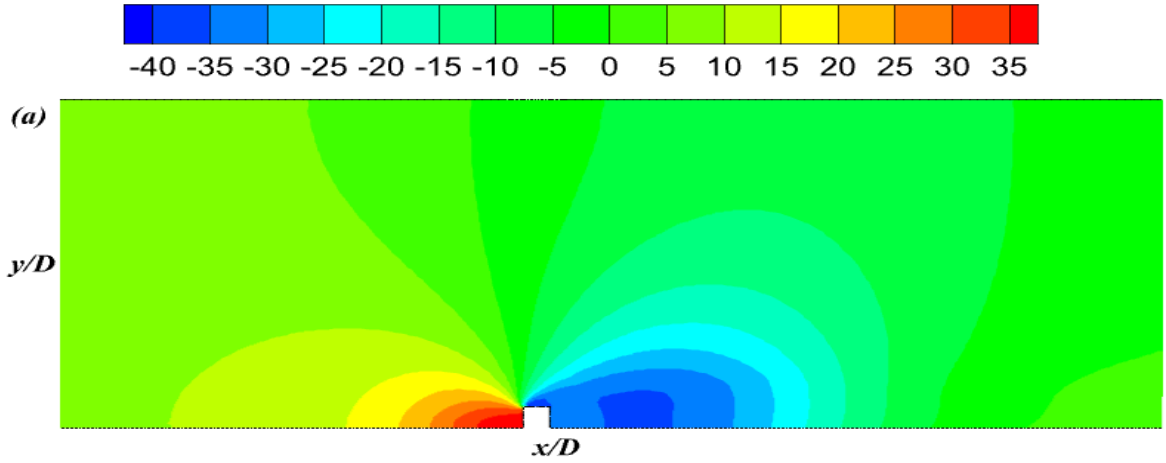

Fig.11: Pressure contour.

The pressure contour illustrates the pressure distribution around a square block in a flow field. High pressure, represented by red and orange colors, is on the upstream side of the block because fluid particles stagnate as they slow down against the front face of the block. Low pressure, indicated by blue and dark blue, exists on the downstream side and in the wake region behind the blockage. Low pressure is caused by flow separation at the sharp edges of the blockage, resulting in wake formation with recirculating flow and lower momentum. Bernoulli's principle also comes into effect, as the fluid accelerates around the edges of the blockage, reducing pressure in these regions. The negative pressure gradient on the upstream side also adds to the deceleration of the fluid and higher pressure at the front face.

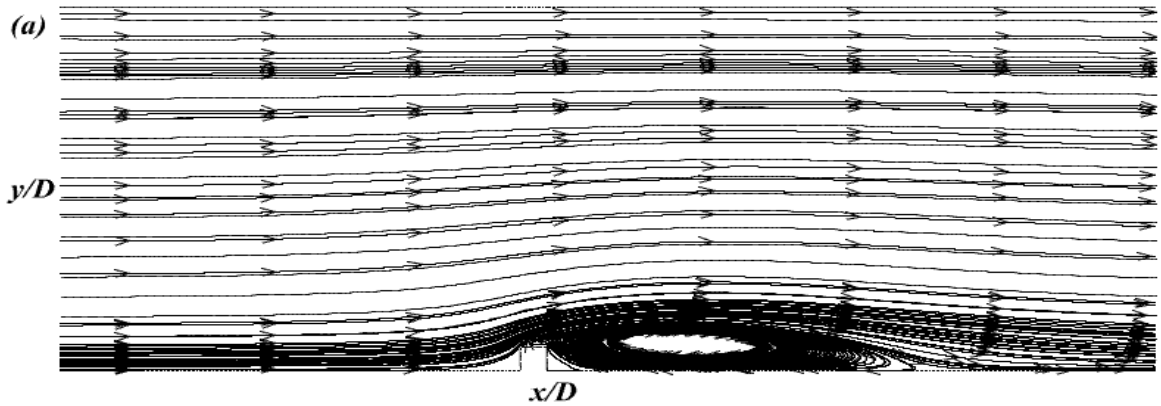

Fig 12. Stream line.

A streamline is a line that is tangent to the velocity vector of a fluid flow at a specific moment. It is a visual representation of the direction a fluid particle would travel at that instant. In the picture you sent, the streamlines illustrate fluid flow around an object.The image illustrates how the streamlines act when fluid passes around a rib. As one gets closer to the object, the streamlines along the surface of the object bend and are compressed. This reflects an increase in velocity and changes in pressure consistent with Bernoulli's principle. Behind the object, the streamlines are irregular, showing turbulence from flow separation. The creation of vortices, or eddies, in this zone consumes energy and forms a pressure gradient, also adding to drag.

4. Conclusion

Numerical simulations in two dimensions have been conducted to analyze the flow dynamics around square wall-mounted structures when exposed to a turbulent boundary layer flow at high Reynolds numbers. The simulations utilize RANS equations, employing the k−ω SST model in conjunction with wall functions. The horizontal velocity profiles at various locations near the square align closely with the experimental results [1], although there is a tendency for overprediction in the freestream region. The validation study indicates that the current numerical model yields satisfactory results when applied to analyze the hydrodynamic characteristics of flow around wall-mounted structures exposed to turbulent boundary layer flow.

References

1. Liu, Y. Z., F. Ke, and Hyung Jin Sung. "Unsteady separated and reattaching turbulent flow over a two-dimensional square rib." *Journal of Fluids and Structures* 24, no. 3 (2008): 366-381.
2. Kuijpers, Antoon, and Tove Nielsen. "Near-bottom current speed maxima in North Atlantic contourite environments inferred from current-induced bedforms and other seabed evidence." *Marine Geology* 378 (2016): 230-236.
3. Gu, Hailin, Jianzhi Yang, and Minghou Liu. "Study on the instability in separating–reattaching flow over a surface-mounted rib." *International Journal of Computational Fluid Dynamics* 31, no. 2 (2017): 109-121.
4. Shi, Liu Liu, Ying Zheng Liu, and Jin Jin Wan. "TR-PIV measurement of separated and reattaching turbulent flow over a surface-mounted square cylinder." *Journal of mechanical science and technology* 24 (2010): 421-428.
5. Menter, Florian R. "Two-equation eddy-viscosity turbulence models for engineering applications." *AIAA journal* 32, no. 8 (1994): 1598-1605.
6. Menter, Florian R., Martin Kuntz, and Robin Langtry. "Ten years of industrial experience with the SST turbulence model." *Turbulence, heat and mass transfer* 4, no. 1 (2003): 625-632.
7. Chiremsel, Rachid, Ali Fourar, Fawaz Massouh, and Zakarya Chiremsel. "CFD analysis of unsteady and anisotropic turbulent flow in a circular-sectioned 90° bend pipe with and without ribs: A comparative computational study." *Journal of Mechanical Engineering and Sciences* 15, no. 2 (2021): 7964-7982.
8. Qian, Suhui, Jicai Zhang, Daosheng Wang, and Ya Ping Wang. "Observational study on drag reduction of continental-shelf bottom boundary layer." *Physics of Fluids* 34, no. 5 (2022).
9. Murakami, Shuzo, S. Iizuka, and Ryozo Ooka. "CFD analysis of turbulent flow past square cylinder using dynamic LES." *Journal of fluids and structures* 13, no. 7-8 (1999): 1097-1112.
10. Murakami, Shuzo, S. Iizuka, and Ryozo Ooka. "CFD analysis of turbulent flow past square cylinder using dynamic LES." *Journal of fluids and structures* 13, no. 7-8 (1999): 1097-1112.